Journal of
Materials Chemistry A

Materials for energy and sustainability

## Accepted Manuscript

This article can be cited before page numbers have been issued, to do this please use: X. Wang, L. Guo, O. Bezsmertna, Y. Wu, D. Makarov and R. Xu, *J. Mater. Chem. A*, 2024, DOI: 10.1039/D4TA02765E.




ROYAL SOCIETY OF CHEMISTRY

rsc.li/materials-a

View Article Online
DOI: 10.1039/D4TA02765E

ARTICLE

Received 00th January 20xx,

# Printed magnetoresistive sensors for recyclable magnetoelectronics

Xiaotao Wang,‡[a] Lin Guo,‡[a] Olha Bezsmertna,[a] Yuhan Wu,[b] Denys Makarov*[a] and Rui Xu*[a]

Accepted 00th January 20xx

DOI: 10.1039/x0xx00000x

We have developed an innovative recyclable printed magnetoresistive sensor using GMR microflakes and AMR microparticles as functional fillers, with PECH as the elastomer binder. Under saturation magnetic fields of 100 mT and 30 mT, these sensors respectively exhibit magnetoresistance values of 4.7% and 0.45%. The excellent mechanical properties and thermal stability of the PECH elastomer binder endow these sensors with outstanding flexibility and temperature stability. This flexibility, low cost, and scalability make these sensors highly suitable for integration into flexible electronic devices, such as smart security systems and home automation. Moreover, these sensors are fully recyclable and reusable, allowing the materials to be separated, reused, and remanufactured without loss of performance. The low energy consumption of the production process and the recyclability of the materials significantly reduce the environmental impact of these magnetic field sensors.

## 1. Introduction

With the development of consumer electronics and Internet of Things (IoT), multifarious electronics have become an indispensable companion of our society, enormously reshaping the way we work, live, entertain, consumption, etc. The rapid expansion of the electronics industry give rise to the skyrocketing volume of electronic waste (e-waste), making it one of the fastest-growing waste streams over the past decades.[1] According to the latest survey report of the United Nations in 2020, about 53.6 million metric tons of e-waste were generated in the global wide in 2019 (approximately 7 kg person-1 year-1), with less than 20% being sent for recycling.[2,3] As a result, many constituent materials, along with all associated inputs in energy and investment, are squandered, leading to resource wastage, shortage of raw materials, and pollution issues.[1–7] The e-wastes have become a significant environmental burden, casting a shadow of immense instability over future development.

As a fundamental component of electronics, magnetic field sensors find wide application in automotive, industry, IoT, biomedicine, consumer electronics,[8–13] benefiting from their capabilities for measuring positions, angles, orientations and movements, as well as touchless interactions characterized by high reliability and sensitivity[14–18]. The typical fabrication process of the magnetic field sensors relies on energy-intensive techniques and expensive facilities, due to the demand of intricate structures necessary for precise sensing capabilities (e.g., multiple nanoscaled stacks for giant magnetoresistance effect).[19–24] Compared with the conventional lithography based fabrication, the energy consumption of printing techniques is substantially lower.[30] The bulky configurations of conventional magnetic field sensors further limit their recycling capability due to the critical requirements for complex processes and harsh treatments (e.g., high temperature, high pressure, combustion, strong acid/alkali, etc).[2,3] In addition, their component materials typically contain hazardous metals of cobalt and nickel and their alloys[22,26–29], which pose potential risks to ecology and public health if not properly recycled. Given that the adverse impacts of magnetic field sensors may arise from the entire lifecycle, holistic considerations should be implemented into different stages of their lifespan.

To address this systemic problem, printed magnetoresistive sensors have been developed to simplify the fabrication process[29–33], thereby reducing energy consumption and equipment investments. Given their susceptibility to mechanical deformation or damage, particularly in applications such as wearable electronics[34,35], self-healing capabilities[36] have been integrated to prolong the operational lifespan of printed magnetic field sensors. However, the challenge of how to handle discarded sensors after their service life, especially in a convenient manner without the assistance of harmful chemicals[32] or harsh treatments[34,35], remains an open question. Considerable efforts have been dedicated to advancing recyclable electronics[37–39]. Although a wide spectrum of recyclable sensors[40,41], transistors[42,43], batteries[44,45], optoelectronic devices[46,47], and generator devices[48–50] have been developed, recycle magnetic field sensors has not been reported yet. To fully mitigate the environmental impacts associated with magnetic field sensors, it is imperative to develop a method that simultaneously reduces energy consumption during initial production and achieves material circularity at the end of their lifecycle.

In this work, we achieved printable magnetic field sensors with full recyclability. To validate the technical feasibility, we printed two types of recyclable sensors with different forms of functional fillers, i.e., giant magnetoresistive (GMR) sensors with $[Co/Cu]_{50}$ multi-stack microflakes and anisotropic magnetoresistive (AMR) sensors with $Ni_{97}Co_3$ microparticles. The polyepichlorohydrin (PECH) elastomer was selected as the polymer binder. It exhibits significant volume shrinkage during solvent evaporation, alongside a high viscosity capable of driving filler movement. These properties work together to guide the rearrangement of fillers, consequently

a. Helmholtz-Zentrum Dresden-Rossendorf e.V., Institute of Ion Beam Physics and Materials Research, Bautzner Landstrasse 400, 01328 Dresden, Germany. Email: r.xu@hzdr.de; d.makarov@hzdr.de

b. School of Environmental and Chemical Engineering, Shenyang University of Technology, Shenyang, China

† Footnotes relating to the title and/or authors should appear here.

Electronic Supplementary Information (ESI) available: [details of any supplementary information available should be included here]. See DOI: 10.1039/x0xx00000x

View Article Online
DOI: 10.1039/D4TA02755E



forming electrical percolation in the printed composites. The formed sensors demonstrate decent magnetoresistance (MR) response with the saturation MR values of about 4.7% at 100 mT for the printed GMR sensors and 0.45% at 30 mT for the printed AMR sensors. Because of the robust electrical pathways, the printed sensors feature low noise and high operational stability. After 1000 cycles of magnetic interaction, their sensing performances have little variation. The thermal stability of PECH endows our sensors with reliable MR response even after exposure to thermal treatments up to 80°C, which is qualified for the requirements as customer electronics. The repeatable dissolution property of PECH allows our samples to be easily decomposed. The fillers inside can be easily extracted from the dissolved polymers via external magnetic fields, and then undergo further processing. By virtue of the energy-effective fabrication and the material circularity that generate a minimal environmental footprint, our sensors exhibit promising potential in IoT applications that require a huge amount of low-cost sensors for real-time information exchange, as evidenced by the implementation of magnetic sensing in smart home systems.

## 2. Experimental section

### 2.1 Printing fabrication of magnetoresistive sensors

The chemicals for the synthesis of the inks, including $Ni_{97}Co_3$ AMR microparticles (Ni 97%/Co 3%, mean particle size of 50 μm), polyepichlorohydrin (Assay 98%), and acetone (Assay ≥ 99.9%), were sourced from Sigma–Aldrich Co. LLC (Fig. S1a). The $[Co/Cu]_{50}$ GMR microflakes were fabricated via magnetron sputtering deposition. Multilayer GMR stacks composed of [Co(1 nm)/Cu(2.2 nm)]$_{50}$ coupled at the 2nd antiferromagnetic maximum were deposited on the AZ 1505 (MicroChemicals GmbH, Germany) coated substrates (Fig. S1b). The $Ni_{97}Co_3$ AMR microparticles and $[Co/Cu]_{50}$ GMR microflakes were used as the AMR and GMR magnetoresistive fillers, respectively. Scanning electron microscopy (SEM) and energy dispersive X-ray (EDX) analysis were performed to investigate the morphology and composition of the magnetoresistive fillers by using the Phenom XL Desktop Scanning Electron Microscope (Thermo Fisher Scientific, United States). The elastomer binder solution consists of polyepichlorohydrin (PECH) and acetone with a mass ratio of 1: 9. The mixture was subjected to stirring at 60°C for 24 hours on a magnetic stirrer hotplate. PECH is a flexible material with an elastic modulus of 0.5 MPa, tensile strength of 17 MPa, and tear strength of 36 $kNm^{-1}$. It remains elastic at low temperatures (glass transition temperature: -14.46°C). It can be dissolved in acetone and other organic solvents and has low toxicity.[55-57] By virtue of these properties, PECH paves the way for applications requiring flexibility, durability, and recyclability. The $Ni_{97}Co_3$ AMR microparticles with a volume ratio of 50% or $[Co/Cu]_{50}$ GMR microflakes with a concentration of 40 mg/mL were incorporated into the elastomer binder to produce printable composites. The mixtures were agitated using a digital vortex mixer (VWR) at 2500 rpm for 60 seconds to ensure homogenous dispersion of functional fillers. The developed composites were printed onto diverse substrates (e.g., FFC cables, commercially available from TME Germany GmbH), followed by drying at room temperature for 180 minutes. For flexible applications, PET films served as the substrate. The electrodes for measurements were pre-deposited on the substrates using electron beam evaporation and the required patterns for the electrodes were defined by the corresponding shadow masks.

### 2.2 Characterization of magnetoresistance and noise for the printed magnetoresistive sensors

The electrical resistances of the printed magnetoresistive sensors were measured on the base of the Kelvin Four-terminal sensing technique, aided with a Tensormeter (HZDR Innovation, Germany). To characterize the noise properties, the electrical resistances of the printed sensors were measured for 30 seconds, with a sampling rate set at 50 Hz. After obtaining the time-based resistance changes, a Fast Fourier Transform (FFT) was applied to calculate the noise spectral density of the signal. All measurements were conducted at room temperature. The MR ratio of the sensor is calculated using the formula MR(H) = [($R(H)$−$R(H$sat))/$R(H$sat)]×100%, where $R(H)$ refers to the resistance value of the sample under the current magnetic field, and $R(H$sat) refers to the resistance value of the sample in the magnetically saturated state. The sensitivity of the sensor is calculated using the formula S(H) = [dR(H)/dH]/R(H), which is defined as the first derivative of the sample's resistance with respect to the external magnetic field divided by the resistance value R(H).

### 2.3 Evaluation of the operational stability for the printed magnetoresistive sensors

For the long-term operation test, the electrical resistance values of the samples were continuously monitored using the Tensormeter. The variations in magnetoresistance across 1000 cycles of magnetic fields was recorded. Regarding the temperature stability, two types of magnetoresistive sensors were subjected to thermal treatments using a hot plate. The sensors were securely mounted on the hot plate, and the temperature settings were adjusted accordingly. Once the hot plate achieved the specified temperatures, each sample was maintained at these temperatures for 10 minutes. Subsequently, the samples were removed and cooled at room temperature for 10 minutes. The Magnetoresistance of each sensor was then measured to assess the effects of thermal exposure. The thermal effects at three temperatures of 40°C, 60°C, and 80°C were systematically evaluated. To assess the mechanical stability, the printed sensors were affixed onto lab-made gadgets with curved surface of various diameters (i.e., 30 mm, 20 mm, and 15 mm). The measured magnetoresistance at the bended states were compared with that for the planar sensor.

### 2.4 Application of the printed magnetoresistive sensors in smart home systems

The flexible sensors printed on the PET foil were affixed to a door handle, with a small magnet positioned nearby on the door. When the handle is rotated, the distance between the sensor and the magnet varies, causing changes in magnetoresistance in response to the fluctuating magnetic fields surrounding the sensors. Real-time signal acquisition was performed using a data acquisition system (DAQ, National Instruments, United States), with the output voltage signals



 

View Article Online
DOI: 10.1039/D4TA02765E

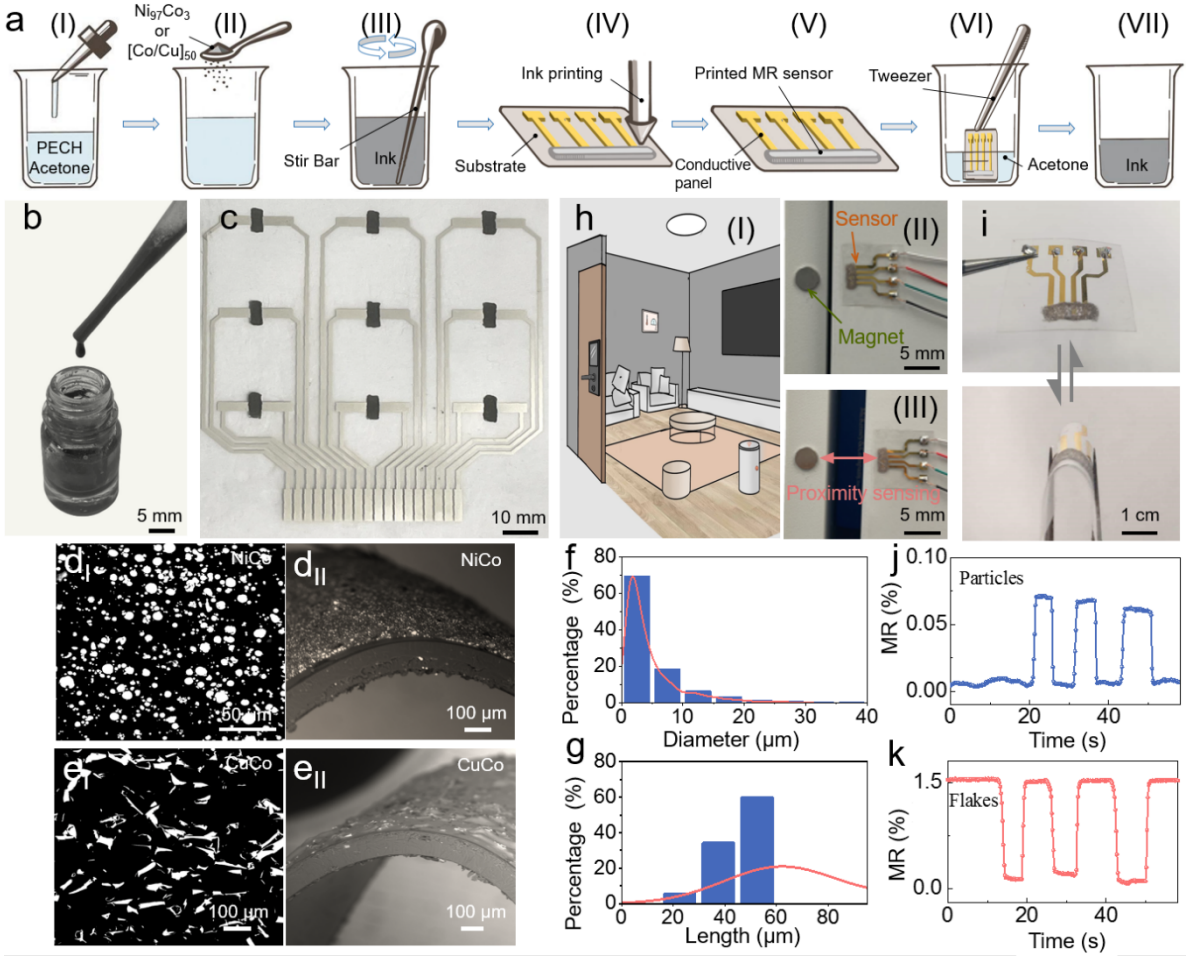


Fig. 1 Recyclable and printable magnetoresistive sensors. (a) Schematic illustration of the fabrication and recycling steps for the printable and recyclable magnetoresistive sensors. ($a_I$) Form binder solutions by dissolving PECH into acetone; ($a_{II}$) Add magnetoresistive fillers into the binder solutions to form printable inks; ($a_{III}$) Stir the ink to ensure uniform distribution of functional fillers; ($a_{IV}$) Print the ink; ($a_V$) Cure the ink to obtain a sensor; ($a_{VI}$) Place the discarded sensor into acetone; ($a_{VII}$) Obtain the new ink. Photographs of (b) the prepared ink and (c) the printed magnetoresistive sensors. SEM images of MR sensors in flat ($d_I$, $e_I$) and bent ($d_{II}$, $e_{II}$) states, based on the material of (d) $Ni_{97}Co_3$ AMR microparticles and (e) $[Co/Cu]_{50}$ multilayer GMR microflakes. Size distribution of (f) AMR microparticles and (g) GMR microflakes. (h) Application of the printed magnetoresistive sensor in smart home. ($h_I$) Schematic illustration; ($h_{II}$, $h_{III}$) Sensor and magnet attached onto furniture surfaces for proximity sensing. (i) Photograph of a printed sensor with mechanical flexibility. Magnetoresistance response of the printed sensors with (j) AMR microparticles and (k) GMR microflakes as fillers.

monitored through LabVIEW software. When the door handle ceased rotation and the output signal stabilized for a duration of three seconds, this stability was interpreted as confirmation of a signal input. The magnitude of the signal was compared against a pre-calibrated value to determine the numerical value entered.

## 3. Results and discussion

### 3.1 Fabrication of recyclable printed magnetoresistive sensors

The printing fabrication of the magnetoresistive sensors are schematically illustrated in Fig. 1$a_{I\text{-}V}$, mainly comprising two steps, i.e., ink preparation and printing. After reaching the end of their lifespan, the printed sensor can be decomposed (Fig. 1$a_{VI\text{-}VII}$), allowing for the retrieval of both the magnetic fillers and dissolved polymeric binders for future processing. To prepare the printable ink, polyepichlorohydrin (PECH) elastomer, serving as the binder, is dissolved into acetone. After complete dissolution, the magnetoresistive fillers are added into the PECH solution. To enhance the printing success rate and performance consistency of the printed sensors, meticulous mixing of the inks before printing is essential, ensuring uniform distribution of the fillers throughout the entire volume (Fig. 1b). Afterwards, the ink is printed onto the substrate with predefined electrodes (Fig. 1c). Following solvent evaporation and consequently a volume shrinkage of 46.7% for the printed composite (Fig. S2), the fillers form electrical pathways within the composite, imparting the printed traces with the ability

View Article Online
DOI: 10.1039/D4TA04215E

to detect magnetic fields. The printed sensors tightly adhere on diverse substrate and the adhesion reliability depends on substrate material, surface roughness, and magnetic filler concentration (Table S1). In contrast to conventional magnetoresistive sensors, which rely on energy-intensive processes and expensive high-vacuum equipment for fabrication, our sensors can be easily processed at room temperature under natural conditions.[21–23,27] This significantly reduces the environmental footprint associated with the fabrication process. Here, $Ni_{97}Co_3$ AMR microparticles (Fig. 1d) or $[Co/Cu]_{50}$ multilayer GMR microflakes (Fig. 1e) are selected to serve as functional fillers to show general applicability of our technique to a wide range of fillers regardless of their compositions, geometries and structural configurations. The GMR microflakes can be sourced from residual waste generated during traditional GMR sensor production, such as GMR microflakes peeled off after photolithography in order to form specific patterns, or remnants left on the inner walls of the sputtering equipment during deposition processes. This approach presents a viable approach to enhance the utilization efficiency of raw materials and effectively transform waste into treasure, thus alleviating environmental burdens. However, the supply of GMR microflake wastes is limited and in small quantities. In order to address the high demand for massive sensor deployment in the IoT era, ensuring a stable, reliable, and cost-effective source of magnetoresistive fillers is crucial. The alternative fillers in the form of AMR microparticles are readily available and require minimal processing, rendering them low-cost, low-energy, and low-carbon-footprint raw materials compared to other fillers with nanoscale characteristics[51,52]. Figure 1j, k records the MR curves of the printed GMR sensor and the AMR sensor during

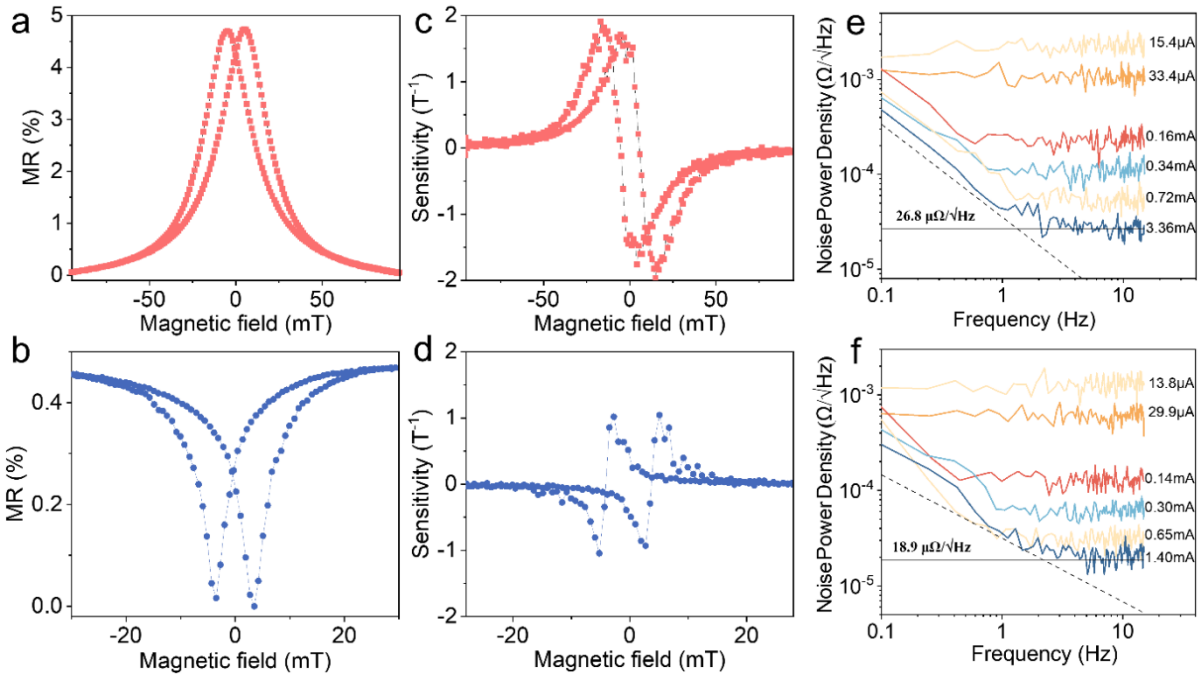


Fig. 2 Magnetoelectric performance of printed magnetoresistive sensors. (a) MR, (c) sensitivity and (e) noise of the printed sensor with $[Co/Cu]_{50}$ GMR microflakes as functional fillers. (b) MR, (d) sensitivity and (f) noise of the printed sensor with $Ni_{97}Co_3$ AMR microparticles as functional fillers. All measurements are performed at room temperature.

magnetic interactions. The successful achievement of stable binding state and electrical percolation in both sensors confirms the extensive compatibility of our technique regardless of the filler dimensions in terms of size and shape (Fig. 1d, e). Adequate material supply, coupled with relatively low environmental impact and cost-effective large-scale manufacturing processes, pave the way for the widespread adoption of magnetic sensors to provide touchless interaction in the IoT applications. For instance, the printed sensors can be seamlessly integrated into household furniture (e.g., doors, drawers) to enable smart home. As magnetic sources approach the sensors (Fig. 1h), their MR exhibit obvious variation. Due to the unique spin-dependent transport properties inherent in multilayer GMR microflakes and AMR microparticles, their MR responses exhibit different trends (i.e., negative and positive changes respectively). The GMR is related to the magnetization direction of the ferromagnetic thin film layers separated by a non-magnetic spacer in the multilayer stack. When the magnetization directions of the neighbouring layers are antiparallel, the resistance value is significantly greater than when the magnetization directions are parallel. The applicability for both two typical morphologies (flakes and particles) also exhibit the technique general utility of the recyclable printed MR sensors based on the PECH elastomer binder. Benefiting from the mechanical flexibility of the binder material PECH, our printed sensors exhibit high resilience (Fig. 1i). This characteristic pave the way for the printed magnetoresistive sensors in emerging applications such as wearable electronics and sticker electronics.

### 3.2 Performance characterization and operational stability test for the printed sensor

To fulfill touchless sensing functionality mentioned above, the magnetoresistance performance and noise characteristics of the printed sensor play critical roles. The magnetoresistance

characterization is carried out with the standard four-point method by measuring the dependence of the electrical resistance variation of the printed active trace on applied magnetic fields. The printed GMR sensor with $[Co/Cu]_{50}$ GMR microflakes as fillers shows a saturation MR of about 4.7% at 100 mT (Fig. 2a). Although the printed AMR sensor with $Ni_{97}Co_3$

AMR microparticles as fillers has lower MR ratios, e.g. with a maximum MR of about 0.45%, its saturation field is reduced to about 30 mT (Fig. 2b). The sensitivity further highlights the distinct operational magnetic field ranges of the two sensors. In the case of the GMR sensor, maximum sensitivity 1.8 $T^{-1}$ is observed at about 15 mT and 3 mT (Fig. 2c), whereas for the AMR sensor, maximum sensitivity 0.9 $T^{-1}$ is observed at about 5 mT and 2 mT (Fig. 2d). By providing a range of operational magnetic fields, our magnetic sensors meet the diverse needs of various applications. These include biomedical devices that operate within narrow magnetic ranges and consumer electronics that necessitate functionality within stronger magnetic fields.[34,53] To further enhance the measurement accuracy of the sensors, it is essential to reduce the hysteresis in the MR curves. Luckily, the flexible fabrication process of our

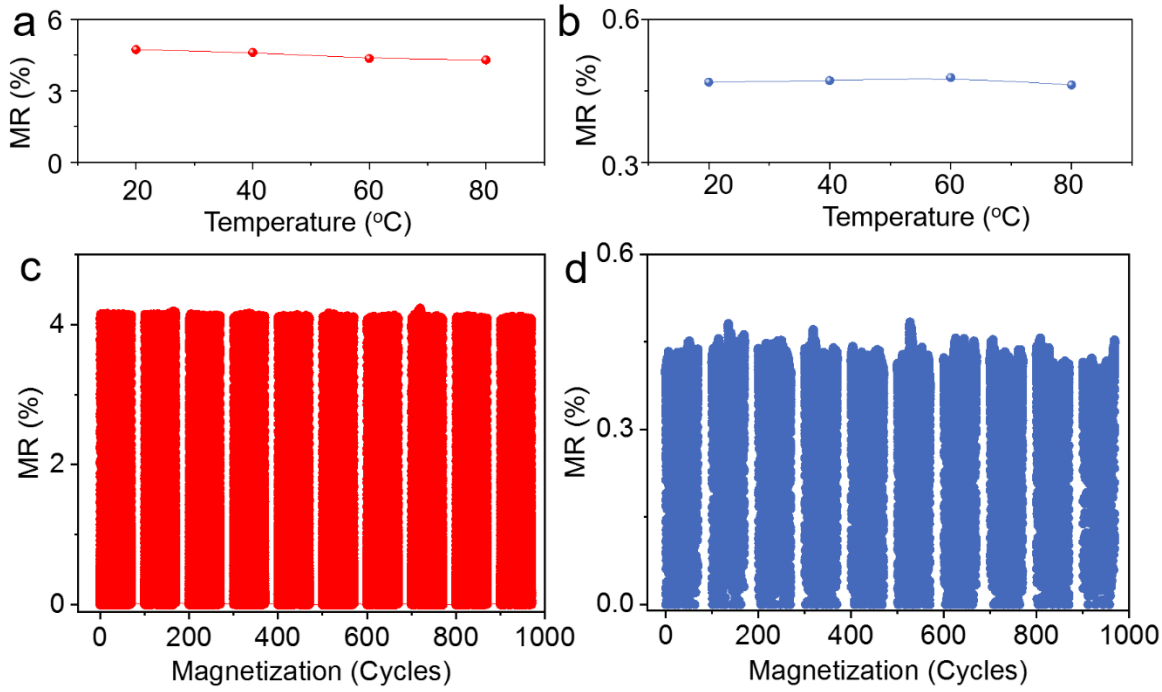


Fig. 3 Operational stability of printed magnetoresistive sensors. The saturation MR values of (a) the printed GMR microflake-based sensors and (b) the AMR microparticle-based sensors after exposure to high temperatures. MR variation of the printed sensors with (c) GMR microflakes and (d) AMR microparticles as fillers during cycled magnetic interaction.

printed sensors are widely compatible with a wide range of fillers, independent of their compositions, geometries and configurations, as well as with various compensation techniques. Therefore, it is believed that by selecting appropriate materials (e.g., soft magnetic materials)[58,59], altering the configuration of the fillers[60,61], inducing bias magnetic field or adding antiferromagnetic to pin the initial magnetic moments in predefined direction with exchange bias effect[62-64], or incorporating compensation techniques[65-67], the printed sensor will be characterized with reduced hysteresis and enhanced accuracy. Signal noise of the printed sensors can undermine their ability to provide accurate and reliable measurements. It directly determines the sensing performance especially for the printed sensors, in which the conductive pathways are made of the fillers, rather than a continuous film. Both types of our sensors exhibit minimal electrical noise, indicating close physical contact between fillers. For example, the noise power density is 26.8 μΩ/√Hz at a current of 3.36 mA and 1.32 Hz for the sensor with GMR microflake fillers (Fig. 2e), and 18.9 μΩ/√Hz at a current of 1.40 mA and 2.18 Hz for the sensor with AMR microparticles fillers (Fig. 2f). These low electrical noises allow the sensors to detect magnetic fields with a maximum resolution of about 0.2 μT and 1.1 μT, respectively, enabling precise measurement in various applications.

In order to evaluate the practical reliability of the printed sensors, we conduct temperature stability tests on their MR performance across a range from room temperature up to 80°C. This temperature range is selected to align with the operational requirements of typical consumer electronics. Our findings reveal that both the printed GMR microflake and AMR microparticle sensors maintain their functionality effectively even after exposure to thermal treatment at 80 °C (Fig. 3a, b). This robustness can be attributed to the low glass transition temperature (-14°C) of the elastomer binder PECH, which

View Article Online
DOI: 10.1039/D4TA02765E



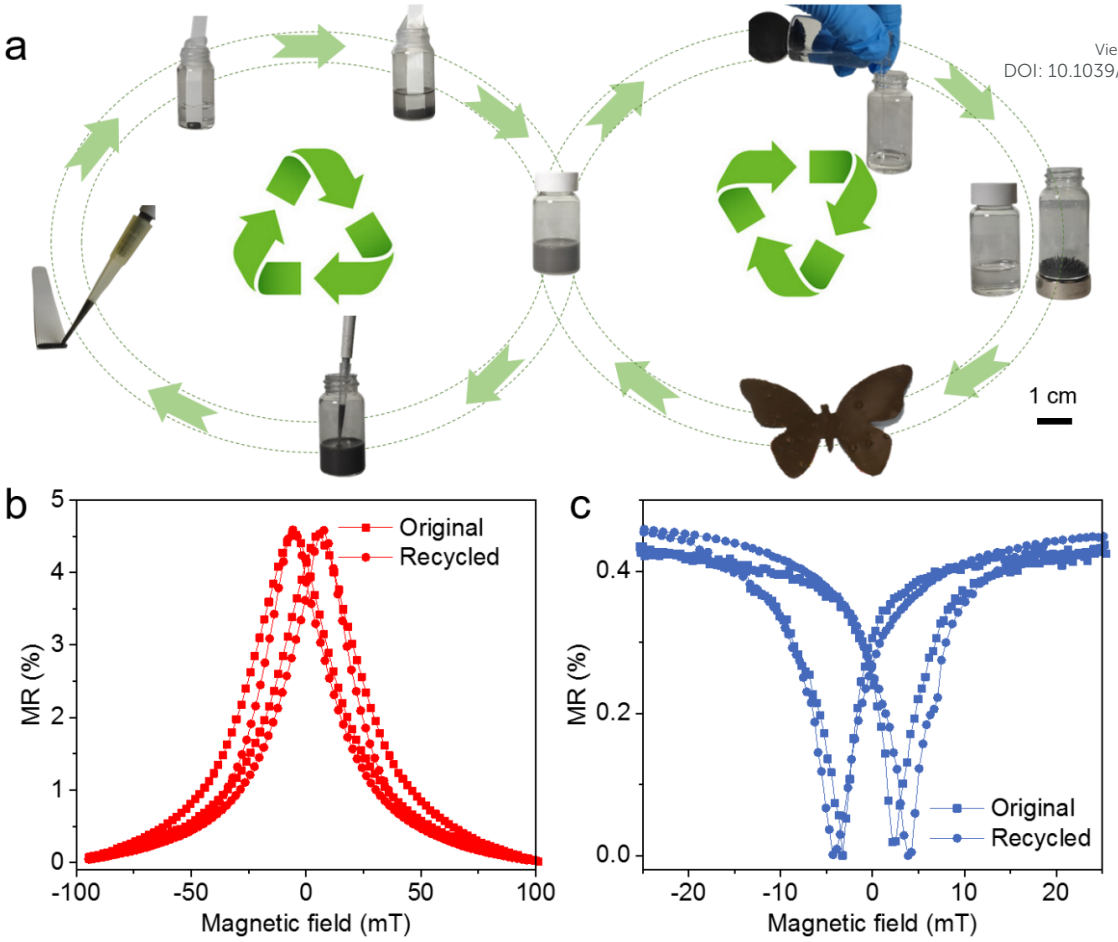


Fig. 4 Recyclable properties of printed magnetoresistive sensors. (a) The left loop illustrates the recycling and reproduction process of printed magnetoresistive sensors: discarded sensors are immersed in solvent to decompose magnetoresistive fillers and polymer binders, after which the recycled ink is used to fabricate new sensors. The right loop illustrates the separation of component materials and the fabrication of a magnetic soft robot using the separated polymers and magnetic fillers. (b,c) MR response of the printed sensors with the recycled materials. The sensors exploit (b) GMR microflakes and (c) AMR microparticles as fillers.

ensures minimal phase change and volume expansion within this temperature regime, thus preserving electrical conductivity. However, we observed a slight degradation in MR performance (less than 9.2%) in the printed GMR microflake samples, which can likely be attributed to the low volume ratio of GMR microflake fillers. Even a minor expansion of the binder can have a notable impact on electric percolation in such cases. Both types of printed sensors demonstrate remarkable stability in repeated magnetic interactions (Fig. 3c, d). No significant performance deterioration was noted after subjecting them to 1000 magnetic cycles, underscoring their robustness and suitability for prolonged use in real-world applications.

### 3.3 Recycling and reprocessing strategies

Once printed magnetoresistive sensors have completed their function or are no longer in use, valuable materials such as polymers and magnetic fillers can undergo a simple recycling process to be reprocessed, as illustrated in the left cycle of Fig. 4a, thereby preventing the generation of new electronic waste. For instance, a certain quantity of discarded sensors is placed into acetone according to the concentration requirements for the new ink. The PECH binder demonstrates excellent solubility in acetone, enabling the sensors to fully decompose within a few minutes, e.g., less than 10 minutes (Fig. S3). The resulting ink can then be utilized to print sensors of various configurations (e.g., size, shape, concentration) to meet diverse practical needs. It's noteworthy that the recycled sensors, whether composed of $[Co/Cu]_{50}$ GMR microflakes (Fig. 3b) or $Ni_{97}Co_3$ AMR microparticles (Fig. 3c), exhibit no performance degradation, even after undergoing multiple recycling and re-fabrication processes (Fig. S4), validating the reliability of our recycling method. This recycling procedure is straightforward and swift, achieving 100% material reuse. If the materials constituting these sensors are not intended for manufacturing sensors again, the recycling strategy can be altered accordingly. Due to their ferromagnetic properties, functional fillers can be effortlessly extracted and separated from the ink. The separated PECH elastomer binder boasts excellent mechanical properties, allowing it to be transformed into magnetic soft robots with self-sensing capabilities by adjusting the filler composition and concentration[54], as depicted in the left cycle of Fig. 4a. Furthermore, the recycled materials can also find utility in other fields such as 3D printing or additive manufacturing. As this technology reduces the demand for raw materials, it holds promise for lowering manufacturing costs and promoting sustainable development.

View Article Online
DOI: 10.1039/D4TA02765E

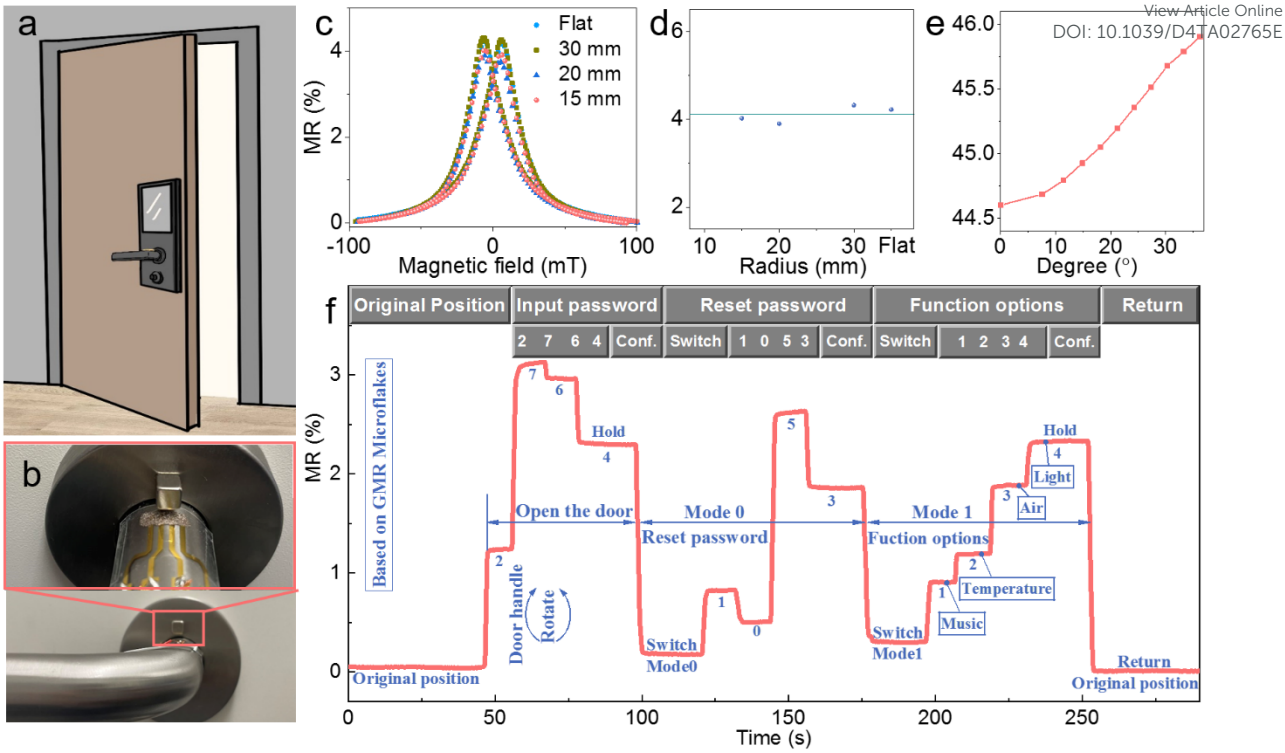


Fig. 5 Sticker electronics application for smart home and security. (a) Schematic illustration and (b) photograph of printed magnetoresistive sensor for the application of sticker electronics in smart home and security. In (b), the printed magnetoresistive sensor adheres conformably to a door handle, which can sense the magnetic fields generated by a permanent magnet placed around the sensor. (c) Magnetoresistance curves and (d) maximum values of printed sensors as bended to different curvatures. (e) Electrical resistance changes in response to the rotation angle of the door handle. As the handle rotates, the spatial position of the sensor relative to the magnet alters, along with the magnetic field experienced by the sensor. (f) Conceptual realization of smart home with a sensor-equipped door handle.

### 3.4 Sticker electronics application for smart home and smart security

By virtue of the aforementioned advantages such as low cost, flexibility, recyclability, temperature stability, and reliability, printed magnetoresistive sensors hold significant promise in the realm of sticker electronics. Here, we showcase the application of printed magnetoresistive stickers in smart security and home automation systems. In our everyday lives, numerous scenarios demand the attachment of electronic devices to curved surfaces (Fig. 5a). Typically, for curved surface applications, electronic devices must undergo specific design and fabrication tailored to each product, given the variations in size and curvature radius of such surfaces. Customized sensors entail high costs and inconvenience for users. The outstanding flexibility of printed magnetoresistive sensors allows for their pre-design and fabrication as flat, sticker-like electronic devices. In practical applications, they can conform precisely to the required shape, maintaining adherence to object surfaces without altering magnetic response performance (Fig. 5c). For instance, we printed a magnetoresistive sensor on a flexible PET substrate serving as a sticker electronic device. We then affixed the sticker to the curved surface of a door handle and secured a permanent magnet on the door (Fig. 5b). Rotating the door handle alters the distance between the magnetoresistive sensor and the permanent magnet, enabling the sensor to detect the rotation state and position of the door handle (Fig. 5d). We encoded the rotation of the door handle using the MR value of the magnetoresistive sensor, dividing the movement of the door handle into different regions and assigning functions such as "0 to 9", "Reset Password", and "Function Options" (Fig. 5e). If movement within a region persists for more than 3 seconds, it is defined as "confirmation". Following the preset protocol, the magnetoresistive door handle can be utilized in smart security and home automation systems. As shown in Fig. 5f, we demonstrated applications such as inputting and resetting passwords for smart security, as well as controlling music playback, temperature adjustment, air purification, and lighting through door handle rotation for home automation. Considering that opening a door is typically the initial action when entering a room, integrating multifunctional features into the door holds significant potential for enhancing user convenience.

## Conclusions

We have introduced a strategy for recyclable printed magnetoresistive sensors. To validate their practical feasibility, we fabricated two types of sensors using GMR microflakes and AMR microparticles as functional fillers, respectively. They exhibit MR values of 4.7% and 0.45% under saturation magnetic fields of 100 mT and 30 mT, respectively. Thanks to the outstanding mechanical properties and temperature stability of the PECH elastomer binder, our printed magnetoresistive sensors exhibit remarkable flexibility,

enabling operation over a wide temperature range. Due to the advantages of mechanical flexibility, low cost, and mass production capability, these sensors hold tremendous potential in the field of sticker electronics. We exemplify their application in a smart door system, where printed magnetoresistive sensors are utilized for smart security and home automation. While the magnetoresistance performance of our printed sensors may not match that of their thin-film counterparts, their low raw material and manufacturing costs render them valuable for applications where high performance and sensitivity are not paramount but cost-effectiveness is crucial. Leveraging the magnetic properties of the functional fillers and the repeatable solubility of the PECH binder in acetone, our printed magnetoresistive sensors demonstrate excellent recyclable properties: constituent materials can be separated, reused, and refabricated without degradation in magnetoresistance performance. The low energy consumption during fabrication and their recyclable nature hold significant potential for reducing the environmental impact associated with magnetic field sensors. Ultimately, this recycling strategy can be extended to magnetic analogy, such as printed magnets and printed magnetic soft robots.

## Author Contributions

X.W. and L.G. contributed equally to this work. R.X. conceived the concept. X.W. designed and fabricated the sensors and conducted the experiments and data collection. L.G. designed and performed the recycling experiments. X.W., L.G., O. B., Y. W., R. X., D. M. analyzed data. L.G. and R.X. wrote the manuscript with comments from all authors. All co-authors edited the manuscript. D.M. supervised the project.

## Conflicts of interest

There are no conflicts to declare.

## Data availability

The data supporting this article have been included as part of the Supplementary Information.

## Acknowledgements

This work is financially supported in part via the European Union in the frame of the project REGO (grant agreement #101070066) and via the German Research Foundation (DFG) grant MA 5144/28-1. X.W. and L.G. is grateful to the China Scholarship Council (CSC) for the Ph.D. scholarship. The authors thank Conrad Schubert (HZDR) for the deposition of metal layer stacks.

.

## References

1 A. Kumar, M. Holuszko and D. C. R. Espinosa, *Resources, Conservation and Recycling*, 2017, **122**, 32–42.

2 Y. He, M. Kiehbadroudinezhad, H. Hosseinzadeh-Bandbafha, V. K. Gupta, W. Peng, S. S. Lam, M. Tabatabaei and M. Aghbashlo, *Environmental Pollution*, 2024, **342**, 123081. View Article Online DOI: 10.1039/D4TA02765E

3 Z. Yao, M. Reinmöller, N. Ortuño, H. Zhou, M. Jin, J. Liu and R. Luque, *Progress in Energy and Combustion Science*, 2023, **97**,101086.

4 W. Li, Q. Liu, Y. Zhang, C. Li, Z. He, W. C. H. Choy, P. J. Low, P. Sonar and K. Ko, Aung Kyaw, *Advanced Materials*, 2020, **32**, 2001591.

5 M. P. Cenci, T. Scarazzato, D. D. Munchen, P. C. Dartora, H. M. Veit, A. M. Bernardes and P. R. Dias, *Advanced Materials Technologies*, 2022, 7, 2001263.

6 Z. Hui, L. Zhang, G. Ren, G. Sun, H. D. Yu and W. Huang, *Advanced Materials*, 2023, **35**, 2211202.

7 J. A. Chiong, H. Tran, Y. Lin, Y. Zheng and Z. Bao, *Advanced Science*, 2021, **8**, 2101233.

8 L. Pan, Y. Xie, H. Yang, M. Li, X. Bao, J. Shang and R. W. Li, *Sensors*, 2023, **23**, 4083.

9 K. Wu, D. Tonini, S. Liang, R. Saha, V. K. Chugh and J. P. Wang, *ACS Applied Materials and Interfaces*, 2022, **14**, 9945–9969.

10 S. Zuo, H. Heidari, D. Farina and K. Nazarpour, *Advanced Materials Technologies*, 2020, **5**, 202000185.

11 S. Yang and J. Zhang, *Chemosensors*, 2021, **9**, 211.

12 D. Rifai, A. N. Abdalla, K. Ali and R. Razali, *Sensors (Switzerland)*, 2016, **16(3)**, 298.

13 G. Lin, D. Makarov and O. G. Schmidt, *Lab on a Chip*, 2017, **17**, 1884–1912.

14 S. Li, P. Cao, F. Li, W. Asghar, Y. Wu, H. Xiao, Y. Liu, Y. Zhou, H. Yang, Y. Zhang, J. Shang, D. Makarov and R. W. Li, *Nano Energy*, 2022, **92**, 106754.

15 S. Li, Y. Wu, W. Asghar, F. Li, Y. Zhang, Z. He, J. Liu, Y. Wang, M. Liao, J. Shang, L. Ren, Y. Du, D. Makarov, Y. Liu and R. W. Li, *Advanced Science*, 2023, 2304525.

16 J. Ge, X. Wang, M. Drack, O. Volkov, M. Liang, G. Santiago, C. Bermúdez, R. Illing, C. Wang, S. Zhou, J. Fassbender, M. Kaltenbrunner and D. Makarov, *Nature Communications*, 2019, **10**, 4405.

17 G. S. Cañón Bermúdez and D. Makarov, *Advanced Functional Materials*, 2021, **31**, 2007788.

18 J. Zhang, G. Chen, Z. Jin and J. Chen, *Advanced Electronic Materials*, 2024, 2300677.

19 I. Ennen, D. Kappe, T. Rempel, C. Glenske and A. Hütten, *Sensors (Switzerland)*, 2016, **16(6)**, 904.

20 P. N. Granell, G. Wang, G. Santiago, C. Bermudez, T. Kosub, F. Golmar and L. Steren, *npj Flexible Electronics*, 2019, **3**, 3.

21 G. Santiago, C. Bermúdez, H. Fuchs, L. Bischoff, J. Fassbender and D. Makarov, *Nature Electronics*, 2018, **1**, 589–595.

22 P. Makushko, E. S. Oliveros Mata, G. S. Cañón Bermúdez, M. Hassan, S. Laureti, C. Rinaldi, F. Fagiani, G. Barucca, N. Schmidt, Y. Zabila, T. Kosub, R. Illing, O. Volkov, I. Vladymyrskyi, J. Fassbender, M. Albrecht, G. Varvaro and D. Makarov, *Advanced Functional Materials*, 2021, **31**, 2101089.

23 L. M. Loong, W. Lee, X. Qiu, P. Yang, H. Kawai, M. Saeys, J. H. Ahn and H. Yang, *Advanced Materials*, 2016, **28**, 4983–4990.

24 K. Huang, Y. Xie, H. Yang, M. Li, L. Pan, X. Bao, Z. He, W. Li and R. W. Li, *Advanced Materials Interfaces*, 2023, **10**, 202202487.

25 M. Li, H. Yang, Y. Xie, K. Huang, L. Pan, W. Tang, X. Bao, Y. Yang, J. Sun, X. Wang, S. Che and R. W. Li, *Nano Letters*, 2023, **23**, 8073–8080.

26 S. Ota, M. Ono, H. Matsumoto, A. Ando, T. Sekitani, R. Kohno, S. Iguchi, T. Koyama and D. Chiba, *Applied Physics Express*, 2019, **12**, 89–93.

27 G. Santiago, C. Bermúdez, D. D. Karnaushenko, D. Karnaushenko, A. Lebanov, L. Bischoff, M. Kaltenbrunner, J. Fassbender, O. G. Schmidt and D. Makarov, *Science advances*, 2018, eaao2623.

28 Z. Wang, X. Wang, M. Li, Y. Gao, Z. Hu, T. Nan, X. Liang, H. Chen, J. Yang, S. Cash and N. X. Sun, *Advanced Materials*, 2016, **28**, 9370–9377.

29 D. Karnaushenko, D. Makarov, C. Yan, R. Streubel and O. G. Schmidt, *Advanced Materials*, 2012, **24**, 4518–4522.

30 D. Makarov, D. Karnaushenko and O. G. Schmidt, *ChemPhysChem*, 2013, **14**, 1771–1776.

31 D. Karnaushenko, D. Makarov, M. Stöber, D. D. Karnaushenko, S. Baunack and O. G. Schmidt, *Advanced Materials*, 2015, **27**, 880–885.

32 E. S. Oliveros-Mata, C. Voigt, G. S. Cañón Bermúdez, Y. Zabila, N. M. Valdez-Garduño, M. Fritsch, S. Mosch, M. Kusnezoff, J. Fassbender, M. Vinnichenko and D. Makarov, *Advanced Materials Technologies*, 2022, **7**, 2200227.

33 P. Gupta, D. D. Karnaushenko, C. Becker, I. E. Okur, M. Melzer, B. Özer, O. G. Schmidt and D. Karnaushenko, *Advanced Materials Technologies*, 2022, **7**, 2200190.

34 M. Ha, G. S. Cañón Bermúdez, T. Kosub, I. Mönch, Y. Zabila, E. S. Oliveros Mata, R. Illing, Y. Wang, J. Fassbender and D. Makarov, *Advanced Materials*, 2021, **33**, 2005521.

35 E. Sergio, O. Mata, G. Santiago, C. Bermúdez, M. Ha, T. Kosub, Y. Zabila, J. Fassbender and D. Makarov, *Applied Physics A*, 2021, **127**, 280.

36 R. Xu, G. S. Cañón Bermúdez, O. V. Pylypovskyi, O. M. Volkov, E. S. Oliveros Mata, Y. Zabila, R. Illing, P. Makushko, P. Milkin, L. Ionov, J. Fassbender and D. Makarov, *Nature Communications*, 2022, **13**, 6587.

37 M. S. Brown, L. Somma, M. Mendoza, Y. Noh, G. J. Mahler and A. Koh, *Nature Communications*, 2022, **13**, 3727.

38 H. Park, S. Kim, J. Lee, I. Lee, S. Bontapalle, Y. Na and K. Sim, *Nature Electronics*, 2024, **7**, 39–50.

39 C. Shi, Z. Zou, Z. Lei, P. Zhu, W. Zhang and J. Xiao, *Science Advances*, 2020, **6**, eabd0202.

40 M. Tavakoli, P. Alhais Lopes, A. Hajalilou, A. F. Silva, M. Reis Carneiro, J. Carvalheiro, J. Marques Pereira and A. T. de Almeida, *Advanced Materials*, 2022, **34**, 2203266.

41 M. Reis Carneiro, A. T. de Almeida, M. Tavakoli and C. Majidi, *Advanced Science*, 2023, **10**, 2301673.

42 X. Yu, D. Liu, L. Kang, Y. Yang, X. Zhang, Q. Lv, S. Qiu, H. Jin, Q. Song, J. Zhang and Q. Li, *ACS Applied Materials and Interfaces*, 2017, **9**, 15719–15726.

43 R. F. P. Martins, A. Ahnood, N. Correia, L. M. N. P. Pereira, R. Barros, P. M. C. B. Barquinha, R. Costa, I. M. M. Ferreira, A. Nathan and E. E. M. C. Fortunato, *Advanced Functional Materials*, 2013, **23**, 2153–2161.

44 T. Liu, Y. Zhang, C. Chen, Z. Lin, S. Zhang and J. Lu, *Nature Communications*, 2019, **10**, 1965.

45 E. Parvini, A. Hajalilou, P. A. Lopes, A. F. Silva, M. S. M. Tiago, P. M. P. Fernandes, A. T. de Almeida and M. Tavakoli, *Advanced Materials Technologies*, 2023, 2301189.

46 T. Ye, F. Xiu, S. Cheng, C. Ban, Z. Tian, Y. Chen, Y. Ding, Z. Zhen, J. Liu and W. Huang, *ACS Nano*, 2020, **14**, 6707–6714.

47 Y. Yao, Y. Chen, K. Wang, N. Turetta, S. Vitale, B. Han, H. Wang, L. Zhang and P. Samorì, *Science Advances*, 2022, **8**, eabn2225.

48 J. Ahn, J. S. Kim, Y. Jeong, S. Hwang, H. Yoo, Y. Jeong, J. Gu, M. Mahato, J. Ko, S. Jeon, J. H. Ha, H. S. Seo, J. Choi, M. Kang, C. Han, Y. Cho, C. H. Lee, J. H. Jeong, I. K. Oh and I. Park, *Advanced Energy Materials*, 2022, **12**, 2201341.

49 J. Zheng, S. Xu, M. Chen, K. Li, Z. Wang, H. Feng, S. Wang, H. Yu and Z. Li, *Nano Energy*, 2024, **122**, 109288.

50 W. Chen, C. Li, Y. Tao, J. Lu, J. Du and H. Wang, *Nano Energy*, 2023, **116**, 108802.

51 R. Xu, L. Wen, Z. Wang, H. Zhao, G. Mu, Z. Zeng, M. Zhou, S. Bohm, H. Zhang, Y. Wu, E. Runge and Y. Lei, *Advanced Functional Materials*, 2020, **30**, 2005170.

52 R. Xu, Z. Zeng and Y. Lei, *Nature Communications*, 2022, **13**, 2435.

53 S. Mostufa, P. Yari, B. Rezaei, K. Xu and K. Wu, *ACS Applied Nano Materials*, 2023, **6**, 13732–13765.

54 E. S. Oliveros-Mata, R. Xu, L. Guo and D. Makarov, *Physical Review Applied*, 2023, **20**, 060501.

55 J. E. Mark, *Polymer Data Handbook*, 2009, 455.

56 E. *Bakhtiarian* and P. J. Foot, *Polymers and Polymer Composites/Polymers & Polymer Composites*, 2023, **31**, 10.

57 D. He and B. Jiang, Journal of Applied *Polymer Science*, 1993, **49**, 618–619.

58 M. A. Khan, J. Sun, B. Li, A. Przybysz and J. Kosel, *Engineering Research Express*, 2021, **3**, 022005.

59 C. Wang, W. Su, Z. Hu, J. Pu, M. Guan, B. Peng, L. Li, W. Ren, Z. Zhou, Z. Jiang and M. Liu, *IEEE Transactions on Magnetics*, 2018, **54**, 1–3.

60 D. J. Kubinski and H. Holloway, *Journal of Applied Physics*, 1996, **79**, 1661–1663.

61 H. Holloway and D. J. Kubinski, *Journal of Applied Physics*, 1996, **79**, 7090–7094.

62 G. Grandi and M. Landini, *IEEE Transactions on Industrial Electronics*, 2006, **53**, 880–885.

63 N. X. Yang, N. H. Liu, N. Y. Wang, N. Y. Wang, N. G. Dong and N. Z. Zhao, *IEEE Transactions on Applied Superconductivity*, 2014, **24**, 1–5.

64 F. Xie, R. Weiss and R. Weigel, *IEEE Transactions on Industrial Electronics*, 2017, **64**, 710–716.

65 I. Jedlicska, R. Weiss and R. Weigel, *IEEE International Symposium on Industrial Electronics*, 2008, 884-889.

66 I. Jedlicska, R. Weiss and R. Weigel, *IEEE Transactions on Industrial Electronics*, 2010, **57**, 1728–1734.

67 J. Han, J. Hu, Y. Ouyang, S. X. Wang and J. He, *IEEE Transactions on Industrial Electronics*, 2015, **62**, 516–524.

View Article Online
DOI: 10.1039/D4TA02765E

The data supporting this article have been included as part of the Supplementary Information.